Electrical Properties of Boron-doped Diamond MOSFETs with Ozone as Oxygen Precursor for Al_2O_3 Deposition

Jiangwei Liu, Tokuyuki Teraji, Bo Da, and Yasuo Koide

***Abstract*—Boron-doped diamond (B-diamond) metal-oxide-semiconductor (MOS) capacitors and MOS field-effect transistors (MOSFETs) are fabricated and characterized. The Al_2O_3 gate insulator is deposited by an atomic layer deposition technique with ozone as oxygen precursor. Leakage current density for the Al_2O_3 (ozone)/B-diamond MOS capacitor is 2.7×10^{-5} A/cm^2 at –9.0 V. Comparing to the capacitance-voltage curve of the Al_2O_3 (water)/B-diamond MOS capacitor, there are no residual capacitance and improved negative flat band voltage shift for the Al_2O_3 (ozone)/B-diamond MOS capacitor. The Al_2O_3 (ozone)/B-diamond MOSFET operates well with the on/off ratio of around 10^8, which is much higher than that of the previous Al_2O_3 (water)/B-diamond MOSFET. After annealing at 500 ℃ for as long as 10 hours, the Al_2O_3 (ozone)/B-diamond MOSFET can still operate well with the on/off ratio larger than 10^6.**

***Index Terms*—Diamond, Boron-doped, MOS capacitor, MOSFET.**

I. Introduction

Over the last couple of years, wide bandgap semiconductors of SiC, GaN, Ga_2O_3, and diamond are developed to meet requirements of next-generation complementary metal-oxide-semiconductor (CMOS) electronic devices [1-4]. Among them, the diamond has the most excellent intrinsic properties. It has wider bandgap energy (5.47 eV), higher breakdown field (10 MV/cm), larger thermal conductivity (22 W/cm·k), and higher carrier mobilities (4500 cm^2/V·s and 3800 cm^2/V·s for electrons and holes, respectively) [5, 6]. Johnson, Keyes, Baliga, and Baliga high-frequency figure-of-merits of diamond are also much larger than those of other wide bandgap semiconductors [7, 8]. Diamond-based electronic devices are promising for future applications in the fields of high-power, high-frequency, high-temperature, and low power-loss.

In order to push forward the development of diamond-based CMOS electronic devices, the diamond MOS capacitors [9, 10], MOS field-effect transistors (MOSFETs) [11-16], and MOSFET logic circuits [17, 18] were fabricated and improved. By far, most of them were fabricated on *p*-type hydrogen-terminated diamond (H-diamond) channel layers. Two-dimensional hole gases are formed on the surface of the H-diamond due to the existence of carbon-hydrogen bonds and negatively charged acceptors [19].

Drain current (I_D), extrinsic transconductance (g_m), cut-off frequency, and breakdown voltage of the H-diamond-based MOSFETs were reported to be as high as 1.35 A/mm, 206 mS/mm, 70 GHz, and 3326 V, respectively [12-14]. Unfortunately, thermal stability of them is still a big issue and very difficult to be resolved [20]. Recently, novel carbon-silicon bonded diamond MOSFETs were fabricated successfully [21]. They have good thermal stability at the measurement temperature of 400 ℃. On the other hand, some researchers made efforts to fabricate *n*-type phosphorus-doped and *p*-type boron-doped diamond (B-diamond) MOSFETs [22-25]. Although their maximum I_D and g_m were quite lower than those of the H-diamond-based ones due to the high activation energies of dopants, they could operate stably at high annealing temperatures (>500 ℃) [25].

The Al_2O_3 films were employed as the gate insulators for the B-diamond MOSFETs thanks to its high critical breakdown field, high thermal stablility, and large band offsets with diamond [26, 27]. In the previous studies, they were deposited by an atomic layer deposition (ALD) technique with the water vapor as the precursor [23-25, 28]. Good operations for the Al_2O_3 (water)/B-diamond MOS capacitors and MOSFETs were confirmed. However, there were residual capacitance and large negative flat band voltage shift for the capacitance-voltage (*C*-*V*) curves of the MOS capacitors [23, 25]. Meanwhile, the maximum on/off ratio for the B-diamond MOSFETs was only around 5×10^5 [23, 29, 30]. These issues are possibly attributed to the surface defects on the B-diamond and poor interfacial quality for the Al_2O_3 (water)/B-diamond, which would hinder the devices for high-performance power switches and other CMOS digital applications. Since the ozone precursor has more oxidizing ability than the water vapor [31], it could possible improve oxygen surface of the B-diamond and the Al_2O_3/B-diamond interfacial quality.

In this study, the B-diamond MOS capacitors and MOSFETs are fabricated and characterized by employing the ozone precursor for the ALD-Al_2O_3 deposition. Because high-temperature operation for the diamond electronic devices is an important application field, electrical properties of the Al_2O_3 (ozone)/B-diamond MOSFETs after annealing at 500 ℃ for as long as 10 hours will also be confirmed.

This work is supported by the Nanotechnology Platform Program and the KAKENHI Projects (Grant JP20H00313 and Grant JP20H02187), the Ministry of Education, Culture, Sports, and Technology, Japan. (Corresponding author: Jiangwei Liu)

J. Liu, T. Teraji, and Y. Koide are with the Research Center for Functional Materials, National Institute for Materials Science (NIMS), Ibaraki 305-0044, Japan (e-mail: liu.jiangwei@nims.go.jp).

B. Da is with the Research and Services Division of Materials Data and Integrated System, NIMS, Ibaraki 305-0047, Japan.

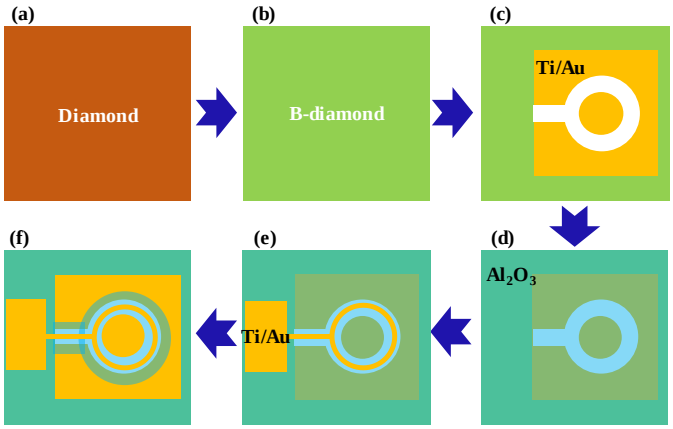

Fig. 1. Fabrication routines for the B-diamond MOSFET: (a) Cleaned diamond, (b) B-diamond growth, (c) Ti/Au Ohmic formation, (d) Al_2O_3 deposition, (e) Ti/Au gate metal formation, and (f) opening windows for Ohmic contact.

II. Experimental

Figure 1 shows the fabrication routines for the circular-type B-diamond MOSFET. The Ib-type (100) diamond substrate was well-polished with root mean square roughness of ~0.1 nm and cleaned in a mixture solution of H_2SO_4 and HNO_3 at 300 ℃ for 3 hours [Fig. 1(a)]. The B-diamond epitaxial layer was grown using a microwave plasma-assisted chemical vapor deposition (MPCVD) technique [Fig. 1(b)]. The microwave power, substrate temperature, and chamber pressure were kept at 1.4 kW, ~1000°C, and 18.6 kPa, respectively. The boron source was not intentionally fed during the diamond growth. Flow rates for the source gases of H_2 and CH_4 were 49 sccm and 1 sccm, respectively [32]. After growth, the B-diamond was treated in the mixture acid solution again to change the hydrogen surface to oxygen. For the circular-type B-diamond MOSFET, the device isolation is not required.

After coating the B-diamond using a spin-coater with a positive photoresist of LOR5A and an image reversal photoresist of AZ5214E sequentially, it was exposed and developed via a scanning maskless lithography system and a TMAH (concentration: 2.38%) solution, respectively. The Ti/Au bilayer (10/150 nm) was evaporated on the B-diamond and annealed at 550 ℃ for 20 minutes to form Ohmic contact via an electron-gun evaporator and a rapid thermal annealing system, respectively [Fig. 1(c)].

The Al_2O_3 gate oxide was deposited using the ALD technique at 200 ℃ with thickness around 24 nm [Fig. 1(d)]. The precursors were $Al(CH_3)_3$ and ozone. The gate metals for the B-diamond MOS capacitors and MOSFETs were Ti/Au bilayer with thicknesses of 10/150 nm [Fig. 1(e)]. The windows of Ohmic contact electrodes were opened by the capacitively coupled plasma reactive-ion etching system in CHF_3+Ar atmosphere [Fig. 1(f)]. Electrical properties of them were measured using a MX-200/B prober and a B1500A parameter analyzer at room temperature.

III. Result and Discussion

A. Thickness and Surface Morphology for B-diamond

Figure 2(a) shows depth profile for concentration of boron atoms in the B-diamond epitaxial layer measured by secondary ion mass spectroscopy (SIMS). Thickness for the B-diamond epitaxial layer is 2000 nm. At the beginning state of its growth, the concentration of boron atoms is as high as 10^{17} cm^3. With the thickness increase, the concentration decreases to be around 4×10^{15} cm^3, which is close to the value in the diamond substrate. At the surface region (~340 nm) of the B-diamond epitaxial layer, the concentration is around 10^{16} cm^3. Because the boron source was not intentionally fed, we can not control the doping concentration very well. Further efforts for the growth of B-diamond epitaxial layer with a stable doping concentration will be performed. The acceptor concentration for the B-diamond epitaxial layer will be deduced by the following capacitance-voltage (*C-V*) measurement.

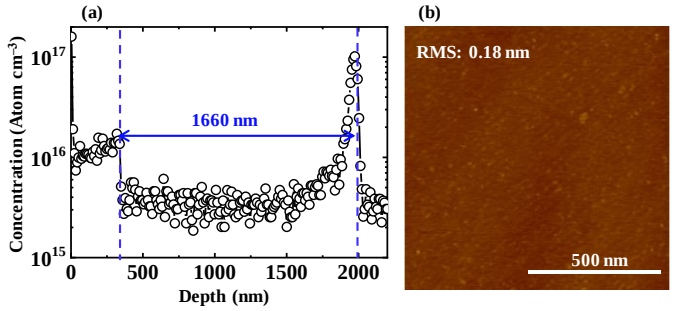

Fig. 2. (a) Depth profile of the SIMS measurement for concentration of boron atoms and (b) AFM image for the B-diamond epitaxial layer.

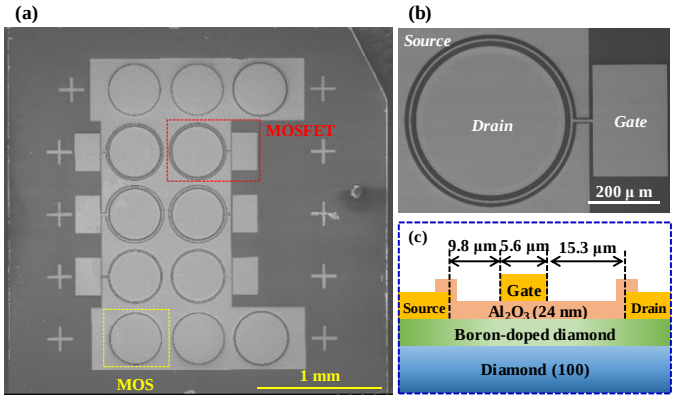

Fig. 3. Scanning electron microscopy image of the entire sample surface. (b) and (c) Image and schematic diagram of the B-diamond MOSFET marked with the red box in Fig. 1(a), respectively.

The atomic force microscopy (AFM) image for the B-diamond epitaxial layer was measured and shown in Fig. 2(b). The root mean square (RMS) value for the 2000 nm-thick B-diamond epitaxial layer is 0.18 nm. It is higher than that (0.15 nm) of the 700 nm-thick B-diamond [33] and lower than that (0.3 nm) of the 30 μm-thick B-diamond epitaxial layer [32].

B. Surface Morphology and Schematic Diagram for B-diamond MOSFETs

Figure 3(a) shows the scanning electron microscopy image of the entire sample surface. The B-diamond MOS capacitors and MOSFETs are fabricated on the same substrate. The diameters for the gate electrodes of the MOS capacitors and drain electrodes of the MOSFETs are the same as 398.2 μm. Figs. 3(b) and 3(c) show the image and schematic diagram of the B-diamond MOSFET marked with the red box in Fig. 1(a), respectively. The gate length is 5.6 μm. Interspace distances for

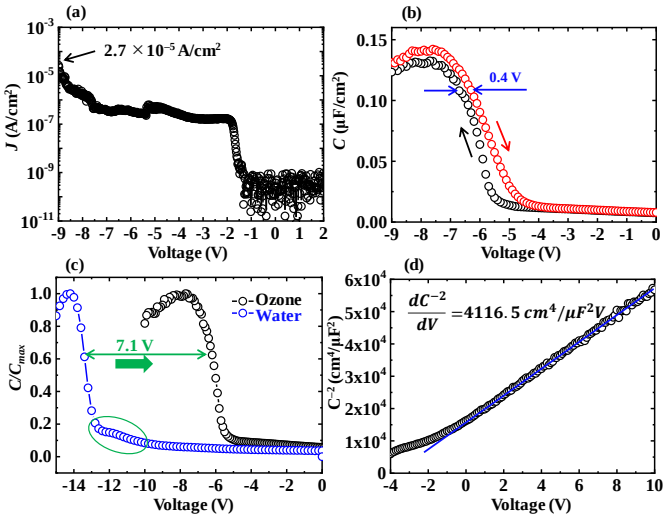

Fig. 4. (a) Leakage current density, (b) *C-V*, (c) C/C_{max}-*V*, and (d) C^{-2}-*V* characteristics for the B-diamond MOS capacitors

gate-to-source and gate-to-drain electrodes are 9.8 and 15.3 μm, respectively. According to the diameter of the gate electrode (398.2 μm), the gate width for the B-diamond MOSFET can be computed to be 1.25 mm.

C. Electrical Properties for B-diamond MOS Capacitor

Figure 4(a) shows leakage current density (*J*) properties for the Al_2O_3 (ozone)/B-diamond MOS capacitor. The variation state of the *J* for the Al_2O_3 (ozone)/B-diamond MOS capacitor is similar with that of the Al_2O_3 (water)/B-diamond MOS capacitor [25]. When the voltage is changing from –1.5 V to –2.0 V, the *J* has a linear relationship with the voltage, which indicates that its conduction mechanism is hopping conduction. With measurement voltage changing from –2.0 V to –9.0 V, the conduction mechanism varies to the Fowler-Nordheim tunneling model [25, 34]. The *J* is 2.7×10^{-5} A/cm^2 at –9.0 V, which is larger than that (<10^{-7} A/cm^2) of the Al_2O_3 (water)/B-diamond MOS capacitor [25]. We have fabricated the Au/Ti/Al_2O_3 (ozone)/Pt/Ti metal-insulator-metal structure to confirm the dielectric constant for the Al_2O_3 (ozone) to be 7.8 at deposition temperature of 200 ºC, which is lower than that of the Al_2O_3 (water) of 8.1 [35]. The dielectric quality of the Al_2O_3 (ozone) is possibly poorer than the Al_2O_3 (water), which leads to the increase of the *J* value. This is possibly attributed to the inadequate reaction between the $Al(CH_3)_3$ and ozone at 200 ºC. Quality of the Al_2O_3 (ozone) film would be further improved by optimizing the deposition conditions in the following study.

Figure 4(b) shows the *C-V* characteristic for the Al_2O_3 (ozone)/B-diamond MOS capacitor. The red and black lines represent the voltage swept from negative to positive and from positive to negative, respectively. The capacitance decreases as the measurement voltage is changing from –8.0 V to –9.0 V. This phenomenon can be ascribed to the increase of the *J*. The maximum capacitance (C_{max}) and hysteresis voltage are 0.142 μF/cm^2 and 0.4 V, respectively. Based on the dielectric constant for the Al_2O_3 (ozone) of 7.8, the capacitance for our 24 nm-thick Al_2O_3 was calculated to be 0.288 μF/cm^2, which is around two times higher than that of the C_{max}. The low C_{max} is possibly attributed to the parallel capacitances between Al_2O_3 insulator and B-diamond semiconductor or the existence of Fermi level pinning effect [36].

Figure 4(c) compared the C/C_{max}-*V* characteristics for the current Al_2O_3 (ozone)/B-diamond (red circle line) and previous studied Al_2O_3 (water)/B-diamond (blue circle line) MOS capacitors [25]. The measurement voltage is swept from positive to negative. For the Al_2O_3 (water)/B-diamond MOS capacitor, large negative flat band voltage shift in the depletion region and residual capacitance at voltage around –12.0 V are observed. These indicate the high positive fixed charge density in the Al_2O_3 (water)/B-diamond MOS capacitor and poor Al_2O_3 (water)/B-diamond interfacial quality. Since there are no above phenomena for the MOS capacitor with the ALD-Al_2O_3 (water) deposited on the H-diamond at 200 ℃ [35], it is natural to believe that the quality of the ALD-Al_2O_3 (water) is good enough for fabricating high-performance B-diamond MOS capacitor. Therefore, the poor C/C_{max}-*V* characteristic for the Al_2O_3 (water)/B-diamond MOS capacitor is mainly attributed to the existence of surface defects on the B-diamond.

On the other hand, no residual capacitance is observed for the *C-V* curve of the Al_2O_3 (ozone)/B-diamond MOS capacitor. Its flat band voltage shift is also much smaller than that for the Al_2O_3 (water)/B-diamond one with the difference between them of 7.1 V. Based on the acceptor density (6.02×10^{15} cm^{-3}) in the B-diamond deduced by the C^{-2}-*V* characteristic [Fig. 4(d)], the Debye length for the B-diamond epitaxial layer can be calculated as 36.7 nm [25]. The flat band capacitance and voltage can be determined to be 0.09 μF/cm^2 and –6.2 V, respectively. Then, the fixed charge density of the MOS capacitor is computed to be 9.2×10^{12} cm^{-2}. It is lower than the value (1.8×10^{13} cm^{-2}) for the Al_2O_3 (water)/B-diamond MOS capacitor [25].

After treating the B-diamond epitaxial layer in the mixture acid solution (H_2SO_4+HNO_3), the surface carbon-hydrogen bonds are modified to carbon-oxygen bonds. However, the coverage of oxygen is only 0.58 monolayer [37] and the carbon dangling bond defects exist on the surface of B-diamond [38, 39]. Since the oxidizing ability of ozone precursor is better than the water vapor [31], it could saturate the carbon dangling bonds and improve the Al_2O_3 (ozone)/B-diamond interfacial quality. The modification of surface defects for the B-diamond with ozone precursor is the possible reasons to make the disappearance of the residual capacitance and the decrease of fixed charge density for the Al_2O_3 (ozone)/B-diamond MOS capacitor.

In this study, the ozone precursor is first supplied in the ALD chamber to oxidize the B-diamond surface. If the B-diamond surface oxidizes first with ozone, then deposits Al_2O_3 film with water precursor, the interfacial quality would be possibly similar with that of the Al_2O_3(ozone)/B-diamond. The residual capacitance for the *C-V* curve of the MOS capacitor would also be improved.

D. Electrical Properties for B-diamond MOSFETs

Figures 5(a) and 5(b) show the I_D–V_D characteristics for the as-fabricated and 500 ºC-annealed B-diamond MOSFETs, respectively. Gate-source voltage (V_{GS}) for both MOSFETs varies from –6.0 to 92.0 V in steps of +2.0 V. Both of them show distinct saturation and pinch-off characteristics. The

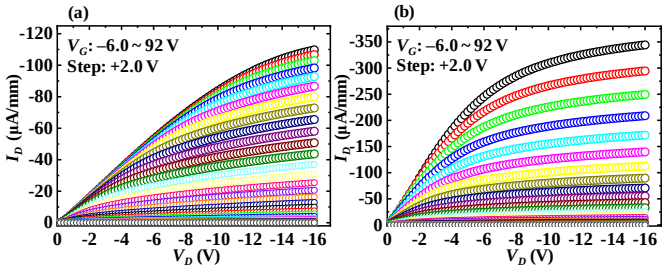

Fig. 5. (a) and (b) I_D–V_D characteristics for as-fabricated and 500 ℃-annealed B-diamond MOSFETs, respectively.

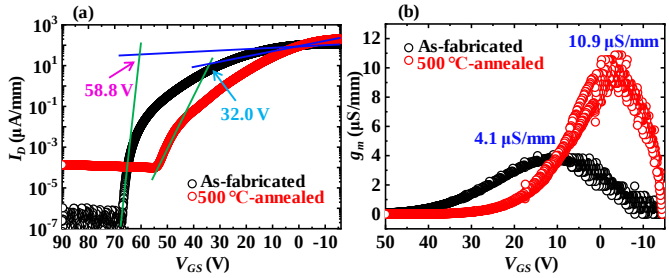

Fig. 6. (a) I_D–V_{GS} and (b) g_m–V_{GS} characteristics for the B-diamond MOSFETs, respectively

maximum I_D values are –109.7 and –344.1 μA/mm, respectively. They are lower than the previous reported value (600 μA/mm) in *Ref.* 25 due to the lower doping concentration for the B-diamond epitaxial layer in this study. There are better linear relationships between the I_D and the low V_D than other previous reports especially as the boron doping concentration lower than 10^{17} cm^{-3} [23, 24]. This indicates that good Ohmic contacts for our B-diamond-based MOSFETs are formed. Their on-resistance values for the as-fabricated and 500 ºC-annealed B-diamond MOSFETs are determined to be 2.2×10^5 and 2.2×10^4 Ω mm, respectively. Annealing at 500 ºC for as long as 10 hours can possible improve the Ohmic contact properties for the Au/Ti and activate the boron dopants for the B-diamond, which would lead to the increase of current output and the decrease of on-resistance for the B-diamond MOSFET.

Figures 6(a) and 6(b) shows the I_D and g_m as functions of V_{GS}, respectively. By a linear extrapolation method, threshold voltage (V_{TH}) values for the as-fabricated and 500 ºC-annealed B-diamond MOSFETs are determined to be 58.8 ±0.1 and 32.0 ±0.1 V, respectively. They are still very large and similar with the previous reports [23-25]. This issue is another important research topic and should be resolved. After annealing, the V_{TH} for the B-diamond MOSFET decreases greatly. This is possibly attributed to that the annealing leads to variation of charges in the Al_2O_3 film and at the Al_2O_3/B-diamond interface.

According to I_D-V_{GS} characteristics, the subthreshold voltage (*SS*) values for the B-diamond MOSFETs before and after annealing were determined to be 414 and 3320 mV/dec, respectively. The interfacial trapped charge density (D_{it}) of the Al_2O_3/B-diamond can be calculated based on the following equation (1).

$$SS = \frac{kT}{q}\ln(10)\left(1+\frac{qD_{it}}{C_{OX}}\right), \quad (1)$$

where the k and T are Boltzmann's constant and room temperature, respectively. C_{OX} is the oxide capacitance of Al_2O_3 film (0.288 μF/cm^2). The D_{it} values were computed as 1.1×10^{13} and 9.9×10^{13} eV^{-1} cm^{-2} for the Al_2O_3/B-diamond interfaces before and after annealing, respectively. Thus, annealing process leads to the degradation of Al_2O_3/B-diamond interfaces. The D_{it} for the Al_2O_3/B-diamond are greater than those for Al_2O_3/H-diamond (6.2×10^{11} eV^{-1} cm^{-2}) [41]. This is attributed to the existence of more defects at the Al_2O_3/B-diamond interface. After annealing at 500 ℃ for as long as 10 hours, the leakage current level at V_{GS} = 90 V increases from 10^{-6} μA/mm to 10^{-4} μA/mm for the Al_2O_3/B-diamond MOSFET. This is possibly ascribed to that the long-term annealing process leads to the quality degradation for the ALD-Al_2O_3 film or the diffusion of gate Ti metal into the Al_2O_3 film.

On/off ratio for the as-fabricated B-diamond MOSFET is around 10^8. It is much larger than those of the Al_2O_3 (water)/B-diamond MOSFETs [23, 29, 30]. This once again approve the improvement of the Al_2O_3/B-diamond interfacial quality by depositing the ALD-Al_2O_3 with the ozone precursor. The high on/off ratio for the Al_2O_3 (ozone)/B-diamond MOSFET makes it suitable for the power switches and other CMOS digital applications. After annealing at 500 ºC for 10 hours, the B-diamond MOSFET still operates stably with the on/off ratio larger than 10^6. This performance is superior to the H-diamond-based MOSFETs [20]. The maximum g_m values are obtained as 4.1 and 10.9 μS/mm for the MOSFETs before and after annealing, respectively, which are the same level with the previous studies [23, 25].

IV. Conclusions

The ALD-Al_2O_3 gate insulator was deposited with the ozone precursor for the B-diamond MOS capacitors and MOSFETs. Comparing to the *C-V* curve of the Al_2O_3 (water)/B-diamond MOS capacitor, there were no residual capacitance and lower negative flat band voltage shift for the Al_2O_3 (ozone)/B-diamond MOS capacitor. There were good operations for the B-diamond MOSFETs even after annealing at 500 ℃ for as long as 10 hours. The maximum I_D and on/off ratio for the as-fabricated B-diamond MOSFET were –109.7 μA/mm and 10^8, respectively. Those for the annealed MOSFET were –344.1 μA/mm and still larger than 10^6, respectively. Improvement of the electrical properties for the B-diamond MOS capacitor and MOSFETs was possibly attributed to the modification of surface carbon dangling bond defects for the B-diamond and the enhancement of Al_2O_3/B-diamond interfacial quality.

References

[1] T. Ueda, "GaN power devices: current status and future challenges," *Jpn. J. Appl. Phys.*, vol. 58, no. SC, p. SC0804, May 2019, doi: 10.7567/1347-4065/ab12c9.

[2] Z. Tong, L. Gu, Z. Ye, K. Surakitbovorn, and J. R. Davila, "On the techniques to utilize SiC power devices in high- and very high-frequency power converters," *IEEE Tran. Power Elect.*, vol. 34, no. 12, pp. 12181–12192, Dec. 2019, doi: 10.1109/TPEL.2019.2904591.

[3] S. J. Pearton, J. Yang, P. H. Cary IV, F. Ren, J. Kim, M. J. Tadjer, and M. A. Mastro, "A review of Ga_2O_3 materials, processing, and devices," *Appl. Phys. Rev.*, vol. 5 no. 1, p. 011301, Jan. 2018, doi: 10.1063/1.5006941.

[4] H. Umezawa, "Recent advances in diamond power semiconductor devices," *Mater. Sci. Semi. Proc.*, vol. 78, pp. 147–156, May 2018, doi: 10.1016/j.mssp.2018.01.007.

[5] J. Isberg, J. Hammersberg, E. Johansson, T. Wikström, D. J. Twitchen, A. J. Whitehead, S. E. Coe, and G. A. Scarsbrook, "High carrier mobility in single-crystal plasma-deposited diamond," *Science*, vol. 297, no. 5587, pp. 1670–1672, Sep. 2002, doi: 10.1126/science.1074374.

[6] C. J. H. Wort and R. S Balmer, "Diamond as an electronic material," *Mater. Today*, vol. 11, no. 1–2, pp. 22–28, Jan./Feb. 2008, doi: 10.1016/S1369-7021(07)70349-8.

[7] B. J. Baliga, "Power semiconductor device figure of merit for high-frequency applications," *IEEE Electron Dev. Lett.*, vol. 10, no. 10, pp. 455–457, Oct. 1989, doi: 10.1109/55.43098.

[8] N. Donato, N. Rouger, J. Pernot, G. Longobardi, and F. Udrea, "Diamond power devices: State of the art, modelling, figures of merit and future perspective," *J. Phys. D: Appl. Phys.*, vol. 53, no. 9, Feb. 2020, Art. no. 093001, doi: 10.1088/1361-6463/ab4eab.

[9] J. Liu, M. Y. Liao, M. Imura, H. Oosato, E. Watanabe, and Y. Koide, "Electrical characteristics of hydrogen-terminated diamond metal-oxide-semiconductor with atomic layer deposited HfO_2 as gate dielectric,"*Appl. Phys. Lett.*, vol. 102, no. 11, pp. 112910-1–112910-4, Mar. 2013, doi: 10.1063/1.4798289.

[10] T. T. Pham, A. Maréchal, P. Muret, D. Eon, E. Gheeraert, N. Rouger, and J. Pernot, "Comprehensive electrical analysis of metal/Al_2O_3/ O-terminated diamond capacitance," *J. Appl. Phys*., vol. 127, p. 161523, Sep. 2018, doi: 10.1063/1.4996114.

[11] W. Wang, Y. Wang, M. Zhang, R. Wang, G. Chen, X. Chang, F. Lin, F. Wen, K. Jia, and H.-X. Wang, "An enhancement-mode hydrogenterminated diamond field-effect transistor with lanthanum hexaboride gate material," *IEEE Electron Dev. Lett.*, vol. 41, no. 4, pp. 585–588, Apr. 2020, doi: 10.1109/LED.2020.2972330

[12] K. Hirama, H. Sato, Y. Harada, H. Yamamoto, and M. Kasu, "Diamond field-effect transistors with 1.3 A/mm drain current density by Al_2O_3 passivation layer," *Jpn. J. Appl. Phys*., vol. 51, no. 9R, p. 090112, Aug. 2012, doi: 10.1143/JJAP.51.090112.

[13] X. Yu, J. Zhou, C. Qi, Z. Cao, Y. Kong, and T. Chen, "A high frequency hydrogen-terminated diamond MISFET with f_T/f_{max} of 70/80 GHz," *IEEE Electron Dev. Lett*., vol. 39, no. 9, pp. 1373–1376, Aug. 2019, doi: 10.1109/LED.2018.2862158.

[14] N. Saha, S. Kim, T. Oishi, and M. Kasu, "3326-V Modulation-Doped Diamond MOSFETs," *IEEE Electron Dev. Lett*., vol. 43, no. 8, pp. 1303–1306, Aug. 2022, doi: 10.1109/LED.2022.3181444.

[15] Z. Ren, J. Zhang, J. Zhang, C. Zhang, S. Xu, Y. Li, and Y. Hao, "Diamond field effect transistors with MoO_3 gate dielectric," *IEEE Electron Dev. Lett.*, vol. 34, no. 6, pp. 786–789, Jun. 2017, doi: 10.1109/LED.2017.2695495.

[16] Z. Yin, M. Tordjman, A. Vardi, R. Kalish, and J. A. del Alamo, "A diamond:H/WO_3 metal–oxide–semiconductor field-effect transistor," *IEEE Electron Dev. Lett.*, vol. 39, no. 4, pp. 540–543, Apr. 2018, doi: 10.1109/LED.2018.2808463.

[17] J. Liu, H. Ohsato, M. Y. Liao, M. Imura, E. Watanabe, and Y. Koide, "Logic circuits with hydrogenated diamond field-effect transistors," *IEEE Electron Dev. Lett.*, vol. 38, no. 7, pp. 922–925, Jul. 2017, doi: 10.1109/LED.2017.2702744.

[18] J. Liu, H. Ohsato, M. Y. Liao, M. Imura, E. Watanabe, and Y. Koide, "Annealing effects on hydrogenated diamond NOR logic circuits," *Appl. Phys. Lett.*, vol. 112, no. 15, p. 153501, April 2017, doi: 10.1063/1.5022590.

[19] C. I. Pakes, J. A. Garrido, and H. Kawarada, "Diamond surface conductivity: Properties, devices, and sensors," *MRS Bulletin*, vol. 39, no. 6, pp. 542–548, June 2014, doi: 10.1557/mrs.2014.95.

[20] J. Liu, H. Oosato, B. Da, T. Teraji, A. Kobayashi, H. Fujioka, and Y. Koide, "Operations of hydrogenated diamond metal–oxide–semiconductor field-effect transistors after annealing at 500 °C," *J. Phys. D: Appl. Phys*., vol. 52, no. 31, p. 315104, May 2019, doi: 10.1088/1361-6463/ab1e31.

[21] T. Bi, Y. Chang, W. Fei, M. Iwataki, A. Morishita, Y. Fu, N. Niikura, and H. Kawarada, "C–Si bonded two-dimensional hole gas diamond MOSFET with normally-off operation and wide temperature range stability," *Carbon*, vol. 175, no. 30, pp. 525-533, April 2021, doi: 10.1016/j.carbon.2021.01.012.

[22] T. Matsumoto, H. Kato, K. Oyama, T. Makino, M. Ogura, D. Takeuchi, T. Inokuma, N. Tokuda, and S. Yamasaki, "Inversion channel diamond metal-oxide-semiconductor field-effect transistor with normally off characteristics," *Sci. Rep.*, vol. 6, p. 31585, Aug. 2016, doi:10.1038/srep31585.

[23] T. T. Pham, J. Pernot, G. Perez, D. Eon, E. Gheeraert, and N. Rouger, "Deep-depletion mode boron-doped monocrystalline diamond metal oxide semiconductor field effect transistor," *IEEE Electron Dev. Lett.*, vol. 38, no. 11, pp. 1571–1574, Nov. 2017, doi: 10.1109/LED.2017.2755718.

[24] T. T. Pham, N. Rouger, C. Masante, G. Chicot, F. Udrea, D. Eon, E. Gheeraert, and J. Pernot, "Deep depletion concept for diamond MOSFET," *Appl. Phys. Lett.*, vol. 111, no. 17, p. 173503, Sep. 2017, doi: 10.1063/1.4997975.

[25] J. Liu, T. Teraji, B. Da and Y. Koide, "Boron-Doped Diamond MOSFETs With High Output Current and Extrinsic Transconductance," *IEEE Tran. Electron Dev.*, vol. 68, no. 8, pp. 3963–3967, Aug. 2021, doi: 10.1109/TED.2021.3087115.

[26] H. C. Lin, P. D. Ye, and G. D. Wilk, "Leakage current and breakdown electric-field studies on ultrathin atomic-layer-deposited Al_2O_3 on GaAs," *Appl. Phys. Lett., vol.* 87, no.18, p. 182904 Sep. 2005, doi: 10.1063/1.2120904.

[27] J. Cañas, G. Alba, D. Leinen, F. Lloret, M. Gutierrez, D. Eon, J. Pernot, E. Gheeraert, and D. Araujo, "Diamond/γ-alumina band offset determination by XPS," *Appl. Surf. Sci.*, vol. 535, no. 15, p. 146301, Jan. 2021, doi: 10.1016/j.apsusc.2020.146301.

[28] K. K. Kovi, Ö. Vallin, S. Majdi, and J. Isberg, "Inversion in metal–oxide–semiconductor capacitors on boron-doped diamond," *IEEE Electron Dev. Lett.*, vol. 36, no. 6, pp. 603–605, June 2015, doi: 10.1109/LED.2015.2423971.

[29] C. Masante, J. Pernot, J. Letellier, D. Eon, and N. Rouger, C. Masante, J. Pernot, J. Letellier, D. Eon, and N. Rouger, "175V, > 5.4 MV/cm, 50 mOhm.cm^2 at 250°C Diamond MOSFET and its reverse conduction," *2019 31st International Symposium on Power Semiconductor Devices and ICs (ISPSD)*, pp. 151–154, May 2019, doi: 10.1109/ISPSD.2019.8757645

[30] C. Masante, N. Rouger, and J. Pernot, "Recent progress in deep-depletion diamond metal–oxide–semiconductor field-effect transistors," *J. Phys. D: Appl. Phys*., vol. 54, no. 23, p. 233002, Mar. 2021, doi: 10.1088/1361-6463/abe8fe.

[31] A. Seweryn, K. Lawniczak-Jablonska, P. Kuzmiuk, S. Gieraltowska, M. Godlewski, and R. Mroczynski, "Investigations of structural and electrical properties of ALD films formed with the ozone precursor, *Materials* vol. 14, no. 18, p. 5395, Sep. 2021, doi: 10.3390/ma14185395.

[32] T. Teraji, T. Yamamoto, K. Watanabe, Y. Koide, J. Isoya, S. Onoda, T. Ohshima, L. J. Rogers, F. Jelezko, P. Neumann, J. Wrachtrup, and S. Koizumi, "Homoepitaxial diamond film growth: High purity, high crystalline quality, isotopic enrichment, and single color center formation," *Physica Status Solidi A*, vol. 212, no. 11, pp. 2365–2384, Oct. 2015, doi: 10.1002/pssa.201532449.

[33] J. Liu, T. Teraji, B. Da, and Y. Koide, "High output current boron-doped diamond metal-semiconductor field-effect transistors," *IEEE Electron Dev. Lett.*, vol. 40, no. 11, pp. 1748–1751, Nov. 2019, doi: 10.1109/LED.2019.2942967.

[34] J. C. Ranuarez, M. J. Deen, and C. H. Chen, "A review of gate tunneling current in MOS device," *Microelectron. Reliab.*, vol. 46, no. 12, pp. 1939-1956, Dec. 2006, doi: 10.1016/j.microrel.2005.12.006.

[35] T. T. Pham, M. Gutiérrez, C. Masante, N. Rouger, D. Eon, E. Gheeraert, D. Araùjo, and J. Pernot, "High quality Al_2O_3/(100) oxygen-terminated diamond interface for MOSFETs fabrication," *Appl. Phys. Lett.* vol. 112, no. 10, p. 102103, Mar. 2018, doi: 10.1063/1.5018403.

[36] J. Liu, H. Oosato, B. Da, and Y. Koide, "Fixed charges investigation in Al_2O_3/hydrogenated-diamond metal-oxide-semiconductor capacitors," *Appl. Phys. Lett.* vol. 117, no. 16, p. 163502 , 2020, doi: 10.1063/5.0023086.

[37] F. N. Li, R. Akhvlediani, M. K. Kuntumalla, and A. Hoffman, "Oxygen bonding configurations and defects on differently oxidized diamond surfaces studied by high resolution electron energy loss spectroscopy and X-ray photoelectron spectroscopy measurements," *Appl. Surf. Sci.* vol. 465, pp. 313-319, Jan. 2019, doi: 10.1016/j.apsusc.2018.09.171.

[38] N. Mizuochi, M. Ogura, J. Isoya, H. Okushi, and S. Yamasaki, "Hydrogen passivation effects on carbon dangling bond defects accompanying a nearby hydrogen atom in p-type CVD diamond," *Physica B: Condensed Matter*. vols. *376-377*, pp. 300–303, April 2006, doi: 10.1016/j.physb.2005.12.077.

[39] N. Mizuochi, M. Ogura, H. Watanabe, J. Isoya, H. Okuchi, and S. Yamasaki, "EPR study of hydrogen related defects in boron-doped p-type CVD homoepitaxial diamond films," *Dia. Related Mater.* vol. 13, no. 11–12, pp. 2096–2099, Nov.-Dec. 2004, doi: 10.1016/j.diamond.2004.06.019.

[40] L. Aarik, H. Mändar, P. Ritslaid, A. Tarre, J. Kozlova, and J. Aarik, "Low-temperature atomic layer deposition of α-Al_2O_3 thin films," *Cryst. Growth Des.* Vol. 21, no. 7, pp. 4220–4229, June 2021, doi: 10.1021/acs.cgd.1c00471.

[41] J. Liu, H. Oosato, B. Da, and Y. Koide, "Investigation of Ohmic contact resistance, surface resistance, and channel resistance for hydrogen-terminated diamond MOSFETs," *IEEE Tran. Electron Dev.*, vol. 69, no. 3, pp. 1181–1186, March 2022, doi: 10.1109/TED.2022.3140699.